Faraday Discuss., 1997, **108**, 255–269

Lattice dynamics from the 'eyes' of the chromophore

Real-time studies of I_2 isolated in rare gas matrices

R. Zadoyan, J. Almy and V. A. Apkarian*

Department of Chemistry, University of California, Irvine, CA 92697-2025, USA

Molecular iodine isolated in rare gas solids is used as a model system to develop the framework for interpretation of condensed phase pump–probe observables, specializing in information content regarding multi-body dynamics. The principles are illustrated through a series of examples, where, beside the molecular vibronic coherence, the cage motions can be directly dissected. The large variety of behaviors which can be staged in this system include: elastic cage recoil, highly non-linear and dissipative cage response, long-lived cage coherence driven through guest–host resonances, nearly decoupled guest–host dynamics, and cage induced dynamical solvation of electronic surfaces. Although the underlying dynamics can be understood in great depth when aided by simulations, we attempt a clear distinction between direct experimental observables and inferences based on simulations.

1 Introduction

The description of the multi-body interactions that control dynamics in condensed media at the atomistic level of detail remains a challenge to modern chemical physics. The slow progress in this field can be attributed to the fact that the standard tools of interrogating intra- and inter-molecular forces and torques, namely spectroscopy and scattering experiments, are blunted by structural and dynamical averaging. This state of affairs is rapidly changing, owing to recent developments in both theoretical and experimental tools. Theoretical methods for explicit computation of observables (quantum correlation functions) for large assemblies are now at hand. More importantly, with the advent of femtosecond laser technologies, the experimental tools for freeze-frame spectroscopy on timescales of elementary processes are becoming commonplace. It is important for observables to be sufficiently detailed to guide theoretical analysis beyond phenomenology. This task, at present, can only be accomplished in model systems. Molecular iodine isolated in a rare gas lattice represents such a model system, one in which laboratory and computer experiments can be applied at a commensurate level of detail. This has been illustrated in the published body of work on this system, where developing theoretical frameworks for understanding the tools of ultrafast pump–probe spectroscopy has been as much an aim as the analysis of the targeted dynamics.[1–10] The combined experimental–theoretical analysis provides dissection of dynamics at unprecedented levels of detail. In this process, however, there is the danger of confusing observables with inferences. Just how much information is directly encoded in the experiment, with regards to the motions of the host, is the subject of this contribution. To this end, we give a systematic development for the bases of interpreting the time dependent resonances observed in pump–probe experiments, what we have referred to in the past as 'dynamical spectra'.[6]

2 Conceptual framework

2.1 Frequency domain spectra reflect quantum correlations

The information content of frequency domain electronic spectra deserves some comment. In condensed media, owing to the large density of states, optical excitations typically create and probe superpositions of states. Since the prepared superpositions evolve during the interrogation, it is more natural to think of spectroscopy as a probe of processes rather than as a probe of states. Accordingly, the more natural language is that of time dependent mechanics; where, for instance, the absorption spectrum, $\sigma(\omega)$, is given as the Fourier transform of the time correlation function, $C(t)$:[11]

$$\sigma(\omega) = \mathrm{Re} \int \exp(i\omega t) C(t) \mathrm{d}t \tag{1a}$$

and

$$C(t) = \sum_i \exp(-\beta E_i) \langle \psi_i(\boldsymbol{r};\, 0) \exp(iH_g\, t/\hbar) \exp(-iH_g\, t/\hbar) \psi_i(\boldsymbol{r};\, 0) \rangle \tag{1b}$$

$C(t)$ is the time dependent overlap between the initial wavefunction of position vector $\boldsymbol{r}$ evolving on excited and ground electronic surfaces.[12] Note that the time dependent many-body wavefunctions, or quantum amplitudes containing phase information, are required for evaluating $C(t)$. Given the large dimensionality of the system, exact treatments are not possible. However, the direct connection between v-domain observables and molecular motions is possible through semiclassical treatments.[4,12–14] We have recently given a practical implementation of such an approach using mixed-order semiclassical initial value propagators in both coordinate and coherent state representation.[13,14] As a concrete example, the $B \leftarrow X$ transition of matrix isolated iodine was considered. This bound-to-bound transition is completely void of structure in condensed media, a result that can be understood in terms of many-body correlations.[13] Although the treatment does not involve separation of coordinates, it is possible to decompose the supersystem correlation function into a product of system and bath (or guest and host) correlations:

$$C(t) = C_Q(t) C_{\{q\}}(t) \tag{2}$$

in which Q is the guest internal coordinate, and $\{q\}$ represents the set of all others. For an absorption spectrum to be structured $C(t)$ must have periodicity, the function must contain recursions. In the present example, the guest frequency is the highest, and therefore should show the shortest recursion, t_Q. However, as it turns out, the bath correlation function decays to zero in a time $t < t_Q$, preempting the possibility of recursions. This very fast decay of the host correlation function is the result of partial loss of joint momentum–coordinate overlap simultaneously along *ca.* 20 degrees of freedom (the impulsively driven cage coordinates). Despite the realism of the simulations, the experiment contains no information past the initial 20 fs of time evolution, the duration of the ballistic escape of the excited state wavefunction out of the Franck–Condon region. This instantaneous decay of information implies that the absorption spectrum can be reproduced by the classical reflection approximation, *i.e.*, by transforming from an initial position distribution to a spectra distribution using the vertical condition for transitions:

$$p(\boldsymbol{r}) \xrightarrow{\delta[\hbar\omega - \Delta V(\boldsymbol{r})]} \sigma(\omega) \tag{3}$$

which is a restatement of the classical Franck principle. Note that in principle this is a multidimensional transformation. However, since the spectrum contains no memory, $p(\boldsymbol{r})$ can be decomposed in terms of a product along any chosen set of coordinates; or,

equivalently, the spectrum $\sigma(\omega)$, can be obtained as the multiple convolution of vertical reflection spectra along individual coordinates. Given that the fact that the vertical $B \leftarrow X$ transition of I_2 leads to a highly repulsive wall, generating a linewidth of *ca.* 2000 cm^{-1} along Q, the effect of the rest of the lattice is to broaden this width by *ca.* 100 cm^{-1}, a barely perceptible effect on the overall shape of the absorption band. Thus, the one-dimensional inversion is wholly adequate, $\sigma(\omega) \leftarrow p(Q)$. We re-emphasize that the loss of information in this case is due to the rapid decay of the bath correlation function, a condition dictated by the details of the dynamics. In contrast, in the case of Cl_2 isolated in solid Ar, the same $B \leftarrow X$ transition leads to a spectrum structured with zero-phonon lines and phonon side-bands,[15] reflecting details of the dynamical coupling between guest and host motions.[14] We should also note that resonant Raman spectra of I_2 in condensed media, which show long progressions, are more informative about the bath correlation function. However, in that case also, the progressions are mainly descriptive of interferences due to simultaneous scattering from B and B′ surfaces, and the information is limited to early time dynamics on the repulsive walls, revealing little specific information regarding lattice motions.[13]

2.2 Ultrafast pump-probe spectra reflect classical correlations

We will concern ourselves in this report with the pump–probe spectroscopy where an ultrashort pulse prepares a superposition state and a second pulse interrogates the system after a time delay. Although formal treatments of this type of spectroscopy exist,[16] logic based on the arguments given in Section 2.1 is sufficient to conclude that where pulses shorter than the characteristic periods of the supersystem are used this type of spectroscopy yields itself to a strictly classical treatment of the matter–radiation interaction. It is well understood that if the pump pulse is short compared to the characteristic periods of the supersystem a wavepacket is prepared. The time evolution of the center of such a packet is the closest approximation to classical mechanical descriptions of microscopic systems. The observable obtained by the probe pulse is the transient absorption spectrum limited to the time window of the probe laser, $I(\omega, t)$, and filtered by its special distribution,

$$\sigma(\omega) = \mathrm{Re} \int \exp(i\omega t) C(t) I(\omega, t) \mathrm{d}t \tag{4}$$

This windowed transform will limit the spectral information content, playing the same role as the bath correlation function, $C_{\{q\}}(t)$ in eqn. (2). Thus, if the pulse width of the laser is shorter than recursion times in the system the transient absorption spectrum is also given by the classical reflection: the probe pulse width limits the correlation time of the evolving packet with its copy on the final electronic surface. Thus, as long as the pump and probe pulses do not overlap in time and are not phase locked, the phase information crucial in the interpretation of frequency domain spectra is inconsequential for time domain pump–probe spectra. The observables can now be simulated through densities, as opposed to amplitudes, and strictly classical treatments are sufficient. In the case of systems involving heavy atoms, such as iodine and krypton, we clearly expect that classical simulations are adequate in describing the molecular dynamics. The pump–probe signal can then be generated from an ensemble of N trajectories by temporal and spectral convolution of the probe laser with the many-body difference potential,

$$S(\tau) = \frac{1}{N} \sum_{i=1}^{N} \int_{-\infty}^{+\infty} \mathrm{d}t \int_{-\infty}^{\infty} \mathrm{d}\omega \, |\mu_{\mathrm{nm}}(\boldsymbol{r}_i)|^2 I_{\mathrm{probe}}(\omega, t; \tau) \delta[\Delta V_{\mathrm{nm}}(\boldsymbol{r}_i, t) - \hbar\omega] \tag{5}$$

in which the indices n and m refer to the initial and final electronic states of the probe transition, τ is the time delay between pump and probe pulses, and the probe pulse is

characterized by the intensity distribution, $I(\omega, t)$. We will commonly make the Condon approximation of ignoring the transition dipole in this development; this in part is justified by the fact that in fixed-color probe experiments localized configurations of coordinates are interrogated. In eqn. (5) we have emphasized that the observable measures the many-body difference potential of the probe transition. This evolves in time. Both the surface on which dynamics occurs and the terminal state used in the transition evolve owing to the motion of the packet. While rigorously correct, the formulation is not very insightful, a number of features being combined in its creation. It is more useful to start with the approximation that the probe configuration is stationary, given by the electronically solvated difference potential, and to then consider deviations from this approximation in terms of dynamical solvation. This allows the definition of a probe window, $W(r, t)$, obtained by transforming the probe spectral distribution to coordinate space:[5]

$$I(\omega, t) \xrightarrow{\delta[\hbar\omega - \Delta V(r)]} W(r, t) \tag{6}$$

The trajectory ensemble then defines the evolving wavepacket, $\rho(r, t)$, and the observable signal is given as the overlap between packet and window,

$$S(\tau) = \int\int \mathrm{d}t\ \mathrm{d}x \rho(r, t) W(r, t, \tau) \tag{7}$$

In eqn. (6) and (7), we have further assumed a one-dimensional reflection to be adequate. Indeed, rather faithful reproduction of experimental signals is obtained,[6] including preparations and interrogations with chirped pulses,[5] by using trajectories obtained classically in full dimensionality, but inverting the data using a window function fixed in coordinate space and localized by the transition dipole on the chromophore. Our main aim in this contribution is to show how this approximation breaks down, where the multidimensional nature of difference potentials becomes evident, and the observables relay information about nuclear solvation. We then consider the detail demanded in constructing the more exact observables, *i.e.*, in describing the time dependent initial and final states.

2.3 Pump–probe resonances yield simultaneous measures of position and momentum

Ultrafast pump-probe signals yield a simultaneous measure of the time dependent position and momentum of a wavepacket. The position is specified through the condition $\delta[\hbar\omega - \Delta V(r)]$, and therefore is contingent on knowledge of the multidimensional difference potentials. The momentum information is encoded in the intensities of observed resonances. This is a direct outcome of eqn. (7), which shows that the signal results from the time overlap between packet and window. This can be analytically shown for a Gaussian packet and pulse, but holds most generally otherwise. Thus, for a packet with instantaneous velocity v:

$$\rho(r, t) = \frac{1}{\sqrt{(2\pi)}\Delta r} \exp\left[- \frac{(r - vt)^2}{2\Delta r^2} \right] \tag{8}$$

and a window function,

$$W(r, t; \tau) = \frac{1}{2\pi\ \delta r\ \delta t} \exp\left[- \frac{(r - r_0)^2}{2\delta r^2} \right] \exp\left[- \frac{(t - \tau)^2}{2\delta t^2} \right] \tag{9}$$

the time dependent signal is obtained as:

$$S(\tau) = \frac{1}{\gamma\sqrt{(2\pi)}} \exp\left[- \frac{(r_0 - v\tau)^2}{2\gamma^2} \right],$$

where

$$\gamma = \sqrt{(\delta r^2 + \Delta r^2 + v^2\ \delta t^2)} \tag{10}$$

The integrated intensity under such a resonance is given as:

$$\int \mathrm{d}\tau S(\tau) = \frac{1}{|v|} \tag{11}$$

Note that the intensity specifies only the magnitude of velocity. The direction of the packet can be obtained when using chirped pulses, where the resonance window evolves in space, when $r_0 = f(t)$ in eqn. (9). A good discussion of this effect has been given elsewhere.[5] Here, suffice it to note that a chirped pulse acquires velocity in coordinate space, and the signal depends on the relative velocity between packet and window. This Doppler effect leads to a narrower but taller resonance peak when the packet and pulse co-propagate, and the opposite effect when they counter-propagate. Thus, by changing the direction of a fixed chirp, it is possible to ascertain direction of the packet's motion. Note that for a given chirp and packet velocity the area under a resonance is conserved.

3 Experimental realizations

The experimental details have been given elsewhere[1–3] and will not be reiterated here. A variety of laser sources are used in these studies, with pump–probe correlation widths ranging from 60 to 150 fs. The fact that the pump and probe pulses are not independently tunable is somewhat limiting. However, given the density of electronic states of iodine, this limitation is not very severe. The latter consideration, along with the consideration that ion-pair states which undergo extensive electronic solvation are commonly used as probe transitions, dictate that the potentials used in the transitions need to be characterized along with the dynamical observables. Below we present data in which the spectral assignments are relatively well determined.

3.1 Momentum transfer to the cage

In solid Kr, the A state of iodine can be prepared near its dissociation limit upon excitation with the fundamental of the Ti : sapphire laser (*ca.* 800 nm); and can be probed *via* the β(1g) ion-pair state using the second harmonic of the laser.[2] The pump–probe signal, the simulated signal, and wavepackets constructed from trajectory swarms are shown in Fig. 1. The signal consists of two resonances arising from the outgoing wavepacket and its return after momentum transfer to the cage. The relative areas of the two peaks are 1 : 2.5, therefore 60% of the initial momentum of the packet is transferred to the cage wall. This is in perfect agreement with the simulated trajectories shown in Fig. 1. The direction of propagation of the packet in this case is rather obvious. This signal has also been used to verify the validity of the chirp diagnostic.[10] Implicit in this simple analysis is the assumption that the packet remains on the same electronic surface: the dynamics is adiabatic at this energy, even though there are some ten molecular states that coalesce at this limit.[17] Note that the analysis is carried out using a window fixed in coordinate space. It is this approximation that allows us to directly read out the information content in the transient. As will generally be the case in condensed phase measurements, the configurations probed, and hence the location of the window, are not available from independent data. They are, however, extractable from the simulations. The trajectories are inverted assuming window parameters r_0 and δr, and then rationalized. The transition can be assigned to the β state minimum, with the conclusion that it is lowered by *ca.* 3600 cm^{-1} through electronic solvation and its bond length has stretched by *ca.* 0.2 Å.[6] It is somewhat surprising that despite this dramatic electronic solvation it is not

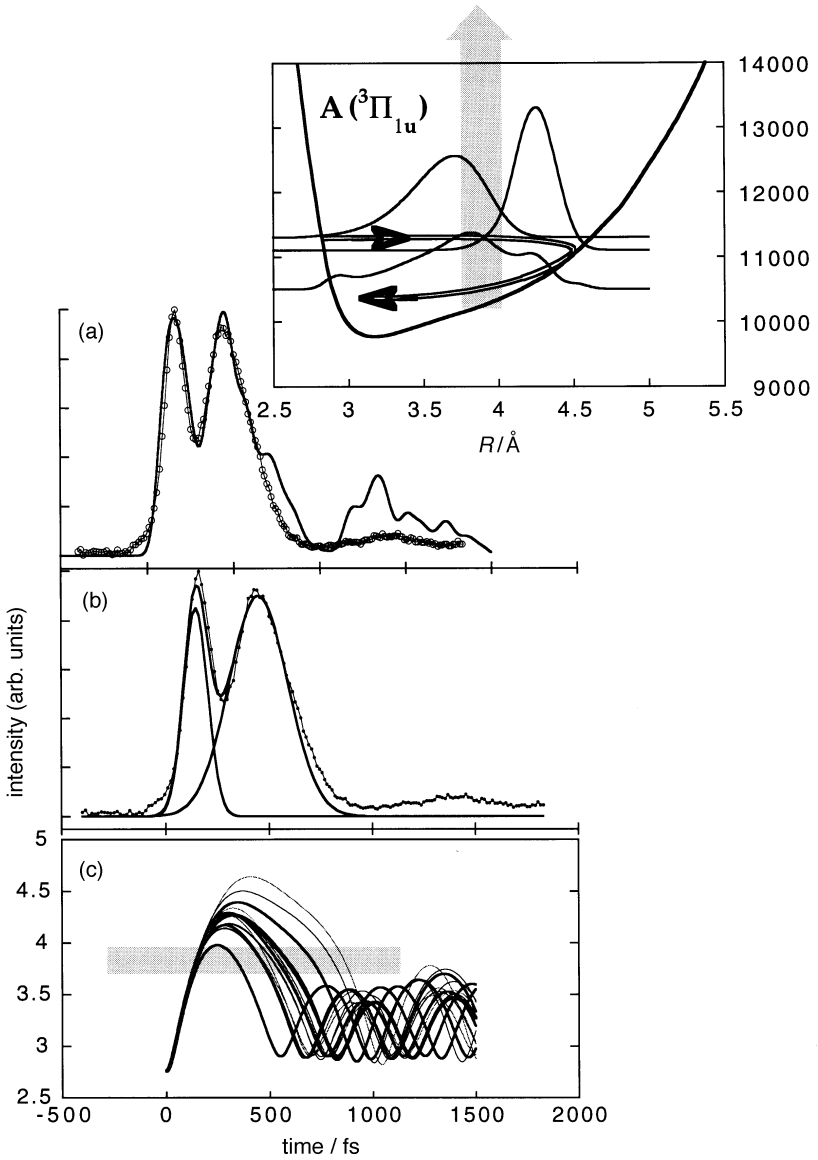

Fig. 1 Momentum transfer to the cage is directly measured by monitoring the pre-collision and post-collision passage of the packet through the probe window. The wavepacket picture is given in the upper right panel, and the probe window is identified by the shaded region. The width of this resonance is due to probing the terminal state, $F(1_g)$, at its minimum. The experimental signal is well reproduced through simulations (a), using the trajectories shown in (c) and a stationary probe window [shaded region in (c)]. The observed resonances can be fitted by a pair of Gaussians, shown in (b), and the relative areas of the Gaussians yield the momenta prior to and after collision.

necessary to assume any nuclear solvation during the process: a window fixed along the I—I bond is assumed in the interpretation. Evidently, the modulation of the ion-pair potential minimum is imperceptible, even though we know that the cage has been set into motion by the impact of the packet (*vide infra*).

3.2 Cage recoil

The same experiment, when repeated at higher energies, 1000–3000 cm^{-1} above dissociation, leads to breaking and cage induced remaking of the I_2 bond.[1,3] An example of the observed pump–probe signal in solid Ar is shown in Fig. 2. These data have previously been analyzed *via* molecular dynamics simulations and the qualitative reproduction of all features has allowed an unequivocal assignment of the resonances to molecular motions.[3] Focus on the peak at a delay of 1.2 ps marked as (4) in Fig. 2. This is clearly shorter than its neighbors on either side, and is a perfectly reproducible feature of the data. Based on eqn. (11), we can immediately conclude that the packet is moving faster in the window than in prior and subsequent periods. Evidently, the molecule was accelerated after being hit by the cage: part of the momentum deposited in the initial crash of the packet with the cage has remained locally and is returned elastically to the molecular coordinate. The timing of this cage recoil is in surprisingly good agrement with the simulations, which make it clear that after the initial collision the fragments lose sufficient energy to fall below the dissociation limit and that the elastic response from the cage at 1.2 ps lifts the molecule above dissociation once again. While the agreement of this detail with the simulations is quite satisfying and has led to confidence in interpretations of other details, we emphasize here the signature of the process in the experimental transient.

The event-by-event analysis of the cage dynamics is useful, particularly since such motions are expected to be rapidly damped. Nevertheless, it is also possible to analyze transients in terms of observable frequencies. For this purpose, only the modulation of the signal is used by subtracting out the incoherent envelope after fitting it to a low order polynomial (see Fig. 3). The oscillations past the recoil are then Fourier transformed to obtain power spectra as a function of excess energy. These spectra contain the lattice frequencies that couple back to the molecular coordinate. The spectra show the

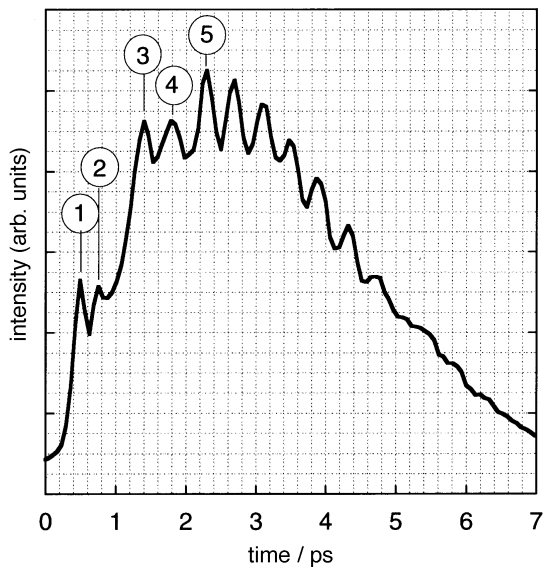

Fig. 2 Breaking and remaking of the I_2 bond on the $A(^3\Pi_{1u})$ surface. Prepared at 720 nm, and probed at 360 nm *via* the $\beta(1_g)$ state. The indicated resonances can be identified as: (1) stretch of the molecular bond; (2) collision of the molecular packet with the cage wall; (3) bond compression; (4) impact of the recoiling cage with the newly formed molecule; (5) first vibration in the bound portion of the molecular potential, followed by coherent vibrations of the remade bond.

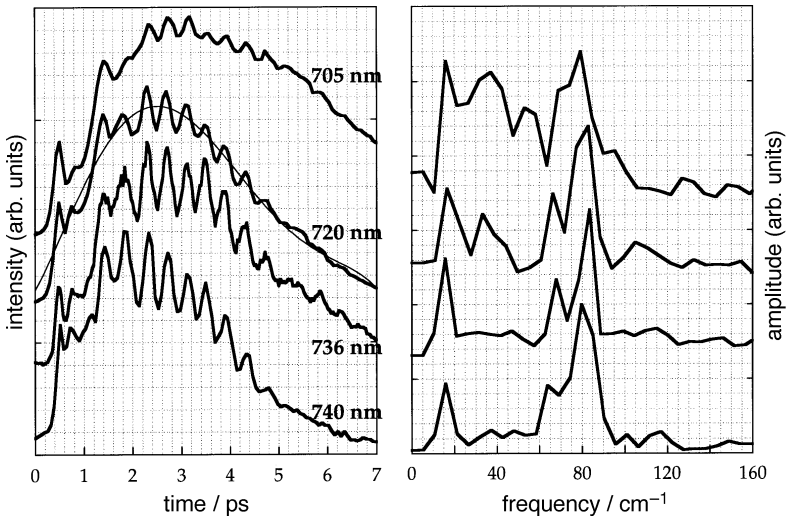

Fig. 3 Cage motions coupled to the chromophore. Left panel: same as in Fig. 2, for different excess energies. The pump wavelengths are indicated, the probe in each case is the second harmonic of the pump. Right panel: power spectra obtained from Fourier transforms of the transients in the left panel. The signal is first fitted with a low order polynomial, as indicated for the 720 nm transient, and only the oscillating part of the signal, past the first recursion at 1.2 ps, is transformed.

red shaded molecular frequency, near 80 cm^{-1}, which is chirped owing to the anharmonicity of the potential. Not surprisingly, in all spectra a shoulder at 65 cm^{-1}, near the Debye limit of solid Ar, can be seen. Further, a frequency near 20 cm^{-1} is common to all excitation energies, and is the only other dominant motion at low excitation energy. This is the mode that contains the elastic response of the cage, the event analyzed above. The elastic distortion of the cage obviously repeats for several periods; the cage reverberates. At higher energies, where the coherences are being lost in the time series, the power spectra indicate that many driven modes of the lattice couple back to the molecular coordinate. Sharp features are not to be expected, since these modes occur in the large density of states of bulk phonons and should rapidly dissipate. Nevertheless, the modes near 45 and 20 cm^{-1} are prominent. Frequency alone cannot identify these modes; simulations must fill the gap. These features reproduced and identified as the E_g 'peanut-distortion' of the cage, where axial atoms stretch while belt atoms compress (the 20 cm^{-1} mode is likely to be shell vibration and the 45 cm^{-1} mode to the radial vibration of the same distortion).

3.3 Linear dissipation, in a silent cage

The B($^3\Pi_{0u}$) state of iodine, which is significantly deeper than the A/A′ states, allows the probing of a wider range of dynamics. When prepared deep in the bound region of the potential, at 545 nm, the molecular vibrational coherence is observed to last for some 15 periods.[6] Moreover, by using chirped pump pulses, it has been shown that the evolving coherence retains memory of the coherence of the radiation field that prepares it.[7] This has been used to argue the feasibility of coherent control of dynamics in condensed media.[7] The data in this case have been quantitatively reproduced by molecular dynamics simulations, again assuming a static window and the classical Franck principle in the inversion of the trajectory data (see Fig. 4).[6,7,9] This success is perhaps the most compelling argument for the general validity of the approach. Note that at simula-

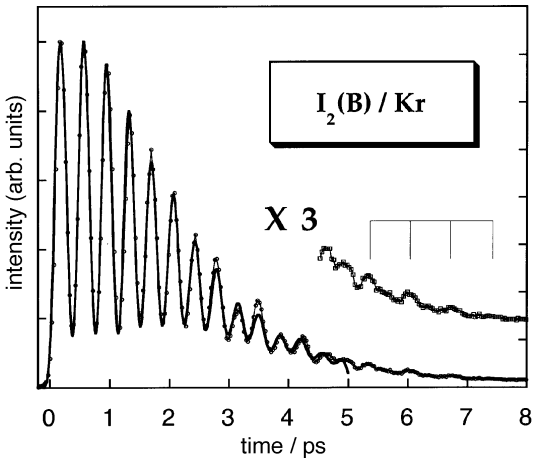

Fig. 4 Quantitative reproduction of the pump–probe signal is possible through classical simulations in the first 5 ps of the transient. At longer times, the signal displays resonances with a period of 700 fs. The data are for excitation deep in the B state, pumped at 549 nm, and probed *via* the $f(0_g)$ ion-pair state.

tion times beyond 5 ps, there are small resonances in the data which were previously ignored. These resonances, which originate from the lattice motions, show a characteristic period of 700 fs (see magnification in Fig. 4). Otherwise, the cage seems to be silent in these transients: the dynamics can be understood as a Morse oscillator in an effective one-dimensional potential which only feels the medium as a linear energy sink. The published data are for solid Kr, and pump/probe combinations of 545/400 nm,[6] or 545 nm/545 nm,[9] with nearly identical results. In the first case, the $F(0_g^+)$ ion-pair state is used as probe, while in the single color experiments the $E(0_g^+)$ ion-pair state is used.

3.4 Long-lived cage coherence driven by a two-to-one resonance

When prepared in the anharmonic part of the B potential, very different behavior is observed. Transients obtained by single color pump–probe measurements in solid Kr are shown in Fig. 5. These transients contain significant information about the cage coherences, which appear as modulation of the signal envelope over the chirped carrier frequency of the I_2 motion. We single out the 515 nm data for dissection. Two sequences are apparent in this transient (see Fig. 6). The first sequence consists of oscillations which start with a period of *ca.* 450 fs and reach a limiting period of *ca.* 350 fs prior to falling out of the observation window. As soon as this progression dies, a new progression with a period of *ca.* 700 fs, the same as that observed in the tail of the 549 nm data, appears. While the first set clearly pertains to the anharmonic I_2 vibration in the B state (gas phase harmonic period of 300 fs), the second set does not correspond to any molecular frequency. The observed constant period of 700 fs corresponds to a frequency of 50 cm^{-1}, which is very close to the Debye limit of solid Kr. These resonances must be ascribed to phonons localized at the impurity site. Note that in these single color measurements the signal must be symmetric about the time origin, a consideration which allows authentication of signal features.

The molecular sequence shows interesting details. The first peak is split into an outgoing wave and a returning wave, as in the case of the A state transient in Fig. 1. However, in contrast with that case, the integrated intensity under the post-collision resonance is smaller than that under the pre-collision resonance. Since the packet is necessarily slower after the collision with the cage, this anomaly cannot be explained

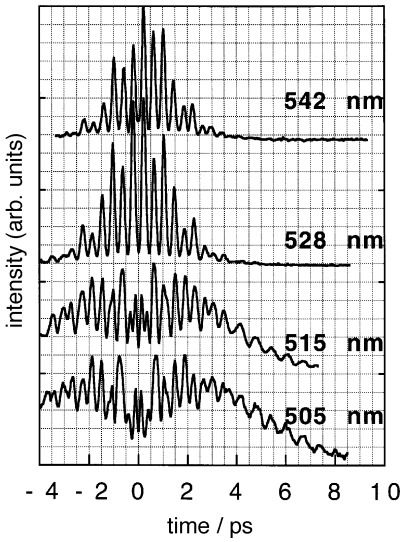

Fig. 5 Single color pump–probe transients: I_2(B) in solid Kr. The modulation of the envelopes in each case is a result of the cage dynamics.

under the assumption of a static probe window. Flux through the probe window must be reduced during the returning packet. Based on the subsequent resonances, since we know that the population remains on the B surface, the only plausible explanation is that the window moves out of the path of the returning packet. This can occur if the probe terminates near the bottom of the ion-pair state, which would be expected to move up in energy by the impact induced dilation of the cage. While this would nicely explain the result, it would necessitate the conclusion that the transients observed at longer wavelengths are from a lower ion-pair state. Under the assumption that the ion-

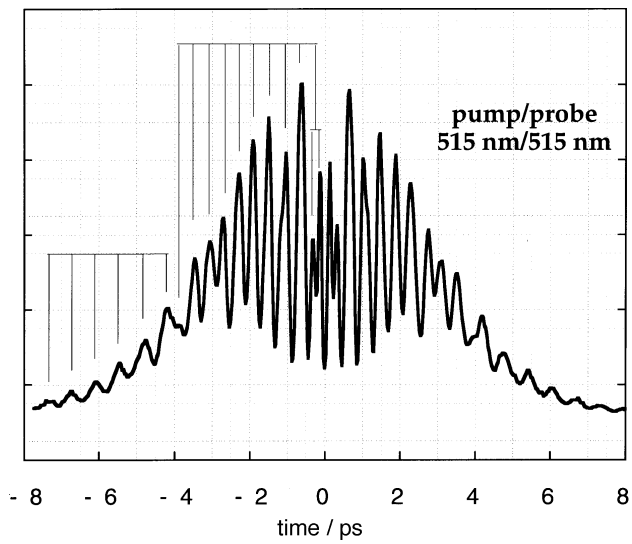

Fig. 6 Dissection of the 515 nm pump–probe signal. Two progressions are observed; the first progression belongs to the I_2 internal vibration (τ = 450–350 fs), while the second is a result of the periodically driven cage motion (τ = 700 fs).

pair states retain their gas phase ordering, it can be concluded that the 545 nm probe reaches the $E(0_g)$ state, and that the 515 nm probe is *via* the $\beta(1_g)$ and therefore a $\Delta\Omega = 1$ transition. All resonances beyond the first form single peaks. The fact that the outgoing and returning packets can no longer be time-resolved necessarily implies that the inner window is now near the outer turning point of the potential.

The third peak in the molecular vibrational sequence, near $\tau = 1$ ps, is shorter than its neigbors and shows a shoulder absent in all others. The reduction of the area under this peak may be ascribed to acceleration of the molecular vibration, due to the impact from the compressing cage. This argument, however, is not sufficient to explain the distortion of the peak. The latter effect again suggests to explain the distortion of the peak. The latter effect again suggests a time dependent probe window, or, equivalently, a difference potential that evolves owing to the dynamics on the B state. This too must be ascribed to solvation dynamics of the ion-pair state. Since this state is strongly solvated, it is expected to be modulated in energy by large amplitude cage motions. In turn the window would be modulated along the molecular coordinate. The distortion of this peak consists of a sharper resonance for the outgoing packet, and a shorter broader rsonance for the incoming packet. Based on the Doppler effect discussed above, we may conclude that the resonance window has acquired velocity along the bond compression direction. Thus, there are two distinct mechanisms at work to produce the distortion of the peak at $\tau \approx 1$ ps: motion of the window due to nuclear solvation and momentum transfer to the molecular coordinate from the elastic response of the cage to the initial impact. Both of these arise from the coherent re-compression of the cage. Note that these features evolve systematically in the set of transients shown in Fig. 5.

We are now in a position to interpret the second sequence of oscillations. The first sequence terminates as the molecular vibrational amplitude is reduced through energy dissipation and the packet no longer reaches the probe window. This is not an abrupt process. In this range of the potential the energy loss is *ca.* 50 cm^{-1} per period,[6] while the probe spectral width is *ca.* 250 cm^{-1}. Modulation of the ion-pair state due to the cage motion will result in modulation of the window along the molecular coordinate, bringing the window into and out of resonance with the characteristic frequency of the coupled local phonon. Given the well defined resonance peaks, this collective mode must be relatively coherent. It is difficult to imagine that such a collective coherence could last for *ca.* 8 ps if it were impulsively created. However, if we note that the observed period is twice that of the molecular vibration, it becomes obvious that the cage coherence is driven by the 2 : 1 resonance between molecule and cage. The observed cage response must be characterized as a periodically driven local phonon. Consideration of structure in the isolation site, and normal mode analysis, identifies this mode as a motion of the belt atoms perpendicular to the molecular axis. This is also observed as the local mode most strongly coupled to the guest vibrations in the case of Cl_2 isolated in Ar, in which the structure and interactions are quite similar to the present case.[14] We resort to molecular dynamics analysis to test the validity of these interpretations.

3.5 Dynamical solvation, multidimensional inversion of trajectory data

Given that the 545 nm data could be simulated quantitatively, it may be surmised that the simulated dynamics on the B state is reliable, that the assumed potential parameters and initial conditions of trajectories are realistic. The novel information in the 515 nm data pertains mainly to the time dependence of the final ion-pair state. We may summarize the implied dynamical solvation of the final state by considering a swarm of trajectories on the B surface and determining the required movement of the window. This is sketched in Fig. 7(a). Quite clearly, non-trivial information concerning the final state energetics is contained in the data. The picture above is the result of the assumption of a probe window based on static difference potentials, which is equivalent to

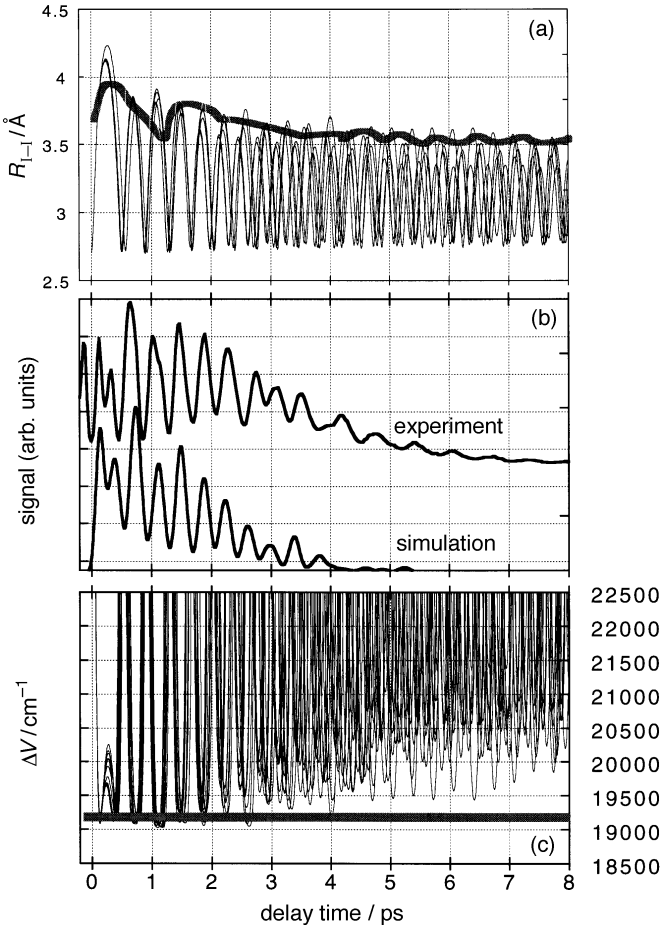

Fig. 7 A comparison between the one-dimensional and many-dimensional approaches to the simulation of the experimental signal. (a) A swarm of I_2 trajectories and a moving window function. (b) The experimentally derived signal (515 nm pump and 515 nm probe), and a signal simulated from the difference potentials in (c). (c) The swarm of difference potentials derived from the trajectories in (a). The thick line represents the probe energy.

one-dimensional inversion of the trajectory data. These considerations do not arise if we explicitly compute the time dependent difference potential and the signal according to eqn. (5). To do this, we have to explicitly evaluate the ion-pair surface as a function of configurations reached during dynamics on the B surface. Given the long-range induction forces that control the solvation of the ionic states, it is not possible to expect a realistic treatment in terms of pair interactions; rather, self-consistent electrostatic expansions are required for the evaluation of energetics.[18] The parameterization of this surface is given in the Appendix.

To simulate the signal, we consider the spectral and temporal overlap of the probe pulse, $I(\omega, t)$, with that of the difference potential, $\Delta V(t)$, as illustrated for a representative swarm in Fig. 7(c). As indicated, the resonance window is now the constant energy line shown. The signal obtained using the independently known parameters of (ω, t) is shown in Fig. 7(b). In this simulation, to produce the best match with experiment, we have allowed constant shifts of energy within *ca.* 400 cm^{-1}, well within the uncertainty

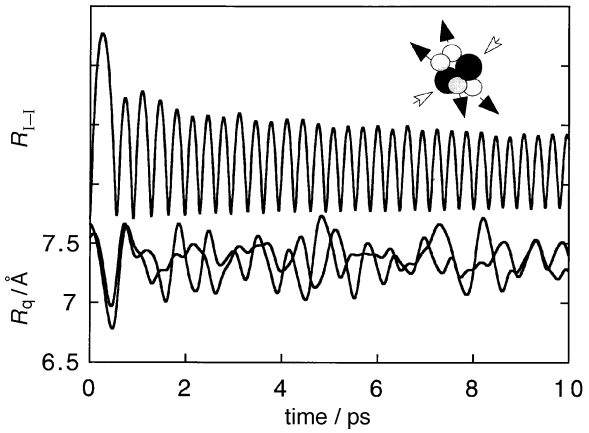

Fig. 8 The 2 : 1 guest–host resonance. A single I_2 trajectory is shown in the upper trace, to compare with frequency of the driven motion of the two coupled Kr pairs. The ordinate is for the internuclear separation of Kr pairs.

of the absolute energy of the computed ionic surface. Among the features reproduced by this simulation are: (a) the splitting of the first peak, and their 'anomalous' relative intensities; (b) the reduction in intensity of the third peak, but not its distortion; (c) the overall envelope of the portion of the signal corresponding to the molecular vibrational sequence. Note that the resonance window in Fig. 7(c) scrapes the difference potential near its minimum, and as already suggested, shows that the 'anomalous' intensity ratio of the split peaks is caused by the recoiling trajectories falling short of the observation window.

The simulated signal also shows some resonances past the main sequence. These are cage induced resonances; however, the driven coherence concluded in Section 3.4 is not reproduced. The 2 : 1 resonance implied by the experiment can be found in individual trajectories, as shown by the example in Fig. 8. Moreover, the driven cage mode that leads to the modulation of ΔV at a period of 700 fs can clearly be identified as the radial motion of the belt atoms, as indicated in the figure. The cap atoms are poorly coupled to the I_2 stretch, because of the oversize cavity created in a divacancy along this axis in Kr. The fact that the sought doubling of the observed modulation period appears in a single trajectory, but not in the ensemble average, implies that the feature is not robust in the simulations and, somewhat surprisingly, it would seem that the simulated system is less coherent than the experiment. The coherence of the guest–host dynamics is sensitively determined by the zero-point amplitudes of the lattice, which dictate the initial conditions of the classical trajectories.[2] The dynamics is particularly sensitive to the impact parameters in the first collision, along the axial direction of the molecule, which entails a rather soft vibrational mode of *ca.* 20 cm^{-1}. The use of a temperature scaled by the Debye frequency of the solid, which we have implemented here as in prior classical simulations of cryogenic solids,[3–9] may not be adequate in this case. Among other reasons for failure to reproduce the cage induced modulation of the signal at long time are the neglect of the transition dipole, the neglect of interactions among the nested manifold of electronic states, and the approximate parametrization of the ionic surface. We cannot yet identify the root cause. Quite clearly, data of the sort presented in the set of Fig. 5 contain features, sufficiently detailed, to warrant attempts at faithful simulations, which would enable a refinement of the many-body energetics and, therefore, dynamics, of both ionic and covalent states. At this stage, the direct interpretation of the experimental transients is the more reliable source of information.

4 Conclusions

We have delineated, through examples, the power of dynamical spectroscopy in unraveling details of multi-body interactions. The model system considered has allowed rigorous development in our understanding of the tool and its observables. This should pave the way to more in-depth analysis of interactions and energetics in systems in which the traditional frequency domain spectroscopies have made very slow progress. The examples we have chosen for this exposition were also devised to illustrate the detailed information contained in the experimental observables. Simulations will remain an inseparable part of such studies; however, it is clear that one can proceed beyond phenomenology, that the experiments can impose sufficient constraints to force precision.

Appendix

The ion-pair potential is described as a sum of electrostatic and covalent-core interactions:

$$V = V_{el} + V_{cc}(\mathrm{Kr—Kr}) + V_{cc}(\mathrm{I^+—Kr}) + V_{cc}(\mathrm{I^-—Kr}) + V(\mathrm{I^+—I^-})$$

where

$$V_{el} = -q \sum_i p_i^{\mathrm{v}} \left(\frac{r_{i,+}^{\mathrm{v}}}{r_{i,+}^3} - \frac{r_{i,-}^{\mathrm{v}}}{r_{i,-}^3} \right) - \sum_{i>j} p_i^{\mathrm{v}} T_{ij}^{\mathrm{t}} p_j^{\mathrm{v}} + \sum_i \frac{p_i^2}{2\alpha}$$

is a sum of charge–induced dipole, induced dipole–induced dipole and polarization self energy, and the core potentials ae taken to be Lennard-Jones, with parameters given below:

$$V_{cc}(\mathrm{Kr—Kr}) = \sum_{i>j} V'(r_{ij}); \quad \sigma = 3.58 \text{ Å}, \varepsilon = 138.93 \text{ cm}^{-1}$$

$$V_{cc}(\mathrm{I^+ - Kr}) = \sum_i V''(r_i); \quad \sigma = 3.6 \text{ Å}, \varepsilon = 130 \text{ cm}^{-1}$$

$$V_{cc}(\mathrm{I^-—Kr}) = \sum_i V'''(r_i); \quad \sigma = 4.0 \text{ Å}, \varepsilon = 160 \text{ cm}^{-1}$$

in which the summation is over all lattice atoms, and $V(\mathrm{I^+—I^-})$ is taken as a Morse function, with parameters $T_e = 41\,411.7 \text{ cm}^{-1}$, $D_e = 30\,750 \text{ cm}^{-1}$, $r_e = 3.647$ Å, and $\beta = 0.56 \text{ Å}^{-1}$. The electrostatic part of the potential is evaluated self-consistently, by the following procedure. The induced polarization at particle i is set proportional to the instantaneous electric field at i,

$$p_i^{\mathrm{v}} = \alpha E_i^{\mathrm{v}} = \alpha \left(\mathrm{e} \frac{r_{i,+}^{\mathrm{v}}}{r_{i,+}^3} - \mathrm{e} \frac{r_{i,-}^{\mathrm{v}}}{r_{i,-}^3} + \sum_j T_{ij}^{\mathrm{t}} p_j^{\mathrm{v}} \right)$$

The electric field at i is found in the computations from the above equation, starting with an initial iteration value based on the pure Coulomb field,

$$E_i^{\mathrm{v}} = e \frac{r_{i,+}^{\mathrm{v}}}{r_{i,+}^3} - e \frac{r_{i,-}^{\mathrm{v}}}{r_{i,-}^3}$$

The explicit self-consistent treatment is limited to 9 shells (66 atoms) and the rest of the extended medium is approximated as a continuum. A correction factor for this truncation, by demanding that the discrete and continuum limits converge, was included. The convergence in p_i^{v} is used as the criterion for self-consistency. After six passes, which is the number of iterations used throughout the simulations, the variation in p_i^{v} is less $1/10^{10}$.

For the covalent surfaces, atom–atom, pairwise additive potentials are used. The I—Kr interactions are treated as Lennard-Jones, using parameters suitable for Xe—Kr. For I_2(B, X) Morse parameters are used.

References

1 R. Zadoyan, Z. Li, C. C. Martens, P. Ashjian and V. A. Apkarian, *Chem. Phys. Lett*., 1994, **218**, 504.
2 R. Zadoyan, Z. Li, C. C. Martens and V. A. Apkarian, *J. Chem. Phys*., 1994, **101**, 6648.
3 Z. Li, R. Zadoyan, V. A. Apkarian and C. C. Martens, *J. Phys. Chem*., 1995, **99**, 7453.
4 J. W. Che, M. Messina, K. R. Wilson, V. A. Apkarian, Z. Li, C. C. Martens, R. Zadoyan and Y. J. Yan, *J. Phys. Chem*., 1996, **100**, 7873.
5 M. Sterling, R. Zadoyan and V. A. Apkarian, *J. Chem. Phys*., 1996, **104**, 6497.
6 R. Zadoyan, M. Sterling and V. A. Apkarian, *J. Chem. Soc*., *Faraday Trans*., 1996, **92**, 1821.
7 C. J. Bardeen, J. Che, K. R. Wilson, V. V. Yakovlev, V. A. Apkarian, C. C. Martens, R. Zadoyan, B. Kohler and M. Messina, *J. Chem. Phys*., 1997, **106**, 8486.
8 A. V. Beuderskii, R. Zadoyan and V. A. Apkarian, *J. Chem. Phys*., 1997, **107**, 8437.
9 R. Zadoyan, M. Sterling, M. Ovchinnikov and V. A. Apkarian, *J. Chem. Phys*., in press.
10 R. Zadoyan, N. Schwentner and V. A. Apkarian, *Chem. Phys*., submitted.
11 R. Kubo and Y. Toyozawa, *Prog. Theor. Phys*., 1955, **13**, 160.
12 J. Heller, *Acc. Chem. Res*., 1981, **14**, 368; S. Mukamel, *Principles of Nonlinear Optical Spectroscopy*, Oxford University Press, New York, 1995.
13 M. Ovchinnikov and V. A. Apkarian, *J. Chem. Phys*., 1996, **105**, 10 312; 1997, **106**, 5775.
14 M. Ovchinnikov and V. A. Apkarian, *J. Chem. Phys*., 1998, **108**, 2277.
15 V. E. Bondybey and C. Fletcher, *J. Chem. Phys*., 1976, **64**, 3615.
16 See, for example, L. W. Unger and J. A. Cina, *Adv. Chem. Phys*., 1997, **100**, 171.
17 V. Batista and D. Coker, *J. Chem. Phys*., 1997, **106**, 6923.
18 E. L. Pollock and B. J. Alder, *Phys. Rev. Lett*., 1978, **41**, 903.

Paper 7/07018G; *Received* 29*th September*, 1997